



## High inertness of $W@Si_{12}$ cluster toward $O_2$ molecule

S.F. Li<sup>a,\*</sup>, Xinlian Xue<sup>a</sup>, Hao Zhai<sup>a</sup>, Xinchuang Nie<sup>a</sup>, Fei Wang<sup>a</sup>, Q. Sun<sup>a</sup>, Yu Jia<sup>a</sup>, Z.X. Guo<sup>b,\*</sup>, S.A. Shevlin<sup>b</sup>

<sup>a</sup> School of Physics and Engineering, Zhengzhou University, Zhengzhou-450052, PR China

<sup>b</sup> Department of Chemistry, University College London, London WC1H 0AJ, UK

### ARTICLE INFO

#### Article history:

Received 19 December 2011

Received in revised form 17 February 2012

Accepted 3 March 2012

Available online 7 March 2012

Communicated by R. Wu

#### Keywords:

First-principles calculations

$O_2$  adsorption

Transition metal doped silicon cluster

Spin-forbidden reaction

### ABSTRACT

The geometry, electronic structure, and reactivity with  $O_2$  molecules of an isolated  $W@Si_{12}$  cluster have been investigated by first principles simulations. The results confirm that  $O_2$  can weakly adsorb on the HP- $W@Si_{12}$  cage with a binding energy of 0.004 to 0.027 eV.  $O_2$  may dissociate on the cluster by overcoming energy barrier of at least 0.593 eV. However, this is a spin-forbidden reaction, rendering the high inertness of the HP- $W@Si_{12}$  cluster toward  $O_2$ . These results confirm the high inertness of the  $W@Si_{12}$  cluster toward  $O_2$  molecules in ambient conditions, in close agreement with experimental observations of magic cluster of  $W@Si_{12}$ .

© 2012 Elsevier B.V. All rights reserved.

### 1. Introduction

Since the discovery of highly stable cage-like  $C_{60}$  fullerenes [1], the search for carbon-free clusters, such as  $Si_n$  cages, has attracted considerable attention, particularly due to the exceptional prominence of silicon in the microelectronics industry. These  $Si_n$  clusters have been extensively investigated both experimentally and theoretically as potential building blocks for the assembly of highly functional nano-devices [2–7]. Unfortunately, stable cage-like Si structures are difficult to synthesize because  $sp^2$  hybridization, which is essential to induce closed cage structures, is energetically unfavorable in pure Si systems. However, stable Si clusters can be synthesized by the incorporation of suitable foreign atoms to terminate the dangling bonds of Si. For example, external hydrogen atoms are introduced to saturate the dangling bonds, while the  $sp^3$  hybridization is also strengthened [8]. Alternatively, encapsulation of transition metal (TM) has also been used to stabilize size-selected cage clusters, as suggested by the experimental work of Beck [9,10] and later confirmed by theoretical calculations [11]. Subsequently, much effort has been expended on the stabilization of silicon cages with significantly large gaps of the highest occupied and the lowest unoccupied molecular orbitals (HOMO–LUMO) by encapsulation of appropriate TM atoms. For example, formation of stable  $MSi_n^+$  cluster ions ( $n = 9, 11, 12, 13, 14$ ;  $M = Hf, Ta, W, Re, Ir$ , etc.) were studied experimentally by Hiura et al. [12]

and theoretically by Uchida et al. [13], suggesting that the highly stable  $TM@Si_{12}$  is either a TM-encapsulated hexagonal prism (HP) cage [8,12–16] or a less-symmetric four pentagonal face (FPF) cage; the structures can be understood in terms of the electronic shell closure due to the 18- and the 20-electron rules, respectively. Interestingly, Kumar and Kawazoe [11] also reported cubic caged  $TM@Si_{14}$  ( $TM = Fe, Ru, Os$ ) and fullerene-like (F)  $TM@Si_{16}$  ( $TM = Hf, Zr$ ) cages with HOMO–LUMO gaps of about 1.5 eV, and Frank-Kasper (FK) tetrahedral  $TM@Si_{16}$  ( $TM = Ti, Hf$ ) cages with HOMO–LUMO gaps of about 2.35 eV, respectively, an indication of high chemical inertness. To understand the mechanism of the stability of these  $TM@Si_n$  clusters, Khanna et al. [17] and Reveles [18] studied the properties of  $Si_nCr$  clusters ( $n = 11–14$ ),  $TM@Si_{12}$  ( $TM = Sc, Ti, V, Cr, Mn, Fe, Co, Ni$ ) and  $TM@Si_n$  ( $TM = Sc, Ti, V$ ;  $n = 15–17$ ), identifying that their stabilities may be consistent with the 18- or the 20-electron rule. In contrast, a recent systematic density-functional investigation [19] claimed that the stabilities of  $TM@Si_n$  clusters ( $TM = Sc, Ti, V, Cr, Mn, Fe, Co, Ni, Cu, Zn$ ;  $n = 8–16$ ) cannot be simply understood by the electron shell filling (18- or 20-electron) rule. The mechanisms underlying their stability should be further investigated.

It is also of interest to study the stability of these Si-based clusters upon exposure to oxygen. The relative stabilities of free standing  $Si_n$  clusters exposed to oxygen have been extensively studied both experimentally [20,21] and theoretically [6,22]. However, there is a paucity of systematic investigation on the stability of these TM encapsulated  $TM@Si_n$  clusters with respect to oxidation, though the adsorption behavior of  $H_2O$  on Ti-doped  $Si_n$  clusters has been investigated both experimentally and

\* Corresponding authors.

E-mail addresses: sflizzu@zzu.edu.cn (S.F. Li), z.x.guo@ucl.ac.uk (Z.X. Guo).

theoretically [23,24]. The results show that smaller Ti-doped  $\text{Si}_n$  clusters ( $n < 12$ ) with the Ti atom partially obscured by Si atoms is available for reaction with a  $\text{H}_2\text{O}$  molecule, whereas larger  $\text{Ti@Si}_n$  clusters ( $n > 12$ ) are highly inert toward  $\text{H}_2\text{O}$  [24], implying that a steric effect plays a key role in their stabilities.

In these stable  $\text{TM@Si}_n$  clusters,  $\text{TM@Si}_{12}$  was predicted as a cage network with a HP structure [12–17,25]. For instance, a HP-Ta@ $\text{Si}_{12}$  structure was observed by scanning tunneling microscopy (STM) on the Si(111)-(7 × 7) surface. Such HP-TM@ $\text{Si}_{12}$  clusters were studied for the assembly of one-dimensional Si nanowires or nanotubes [26], due to the high stability and high symmetry of the HP configuration. However, some very important questions still need to be addressed, for example: 1) How inert are these  $\text{TM@Si}_{12}$  clusters toward oxidation? 2) What is the process for an  $\text{O}_2$  molecule reacting with the  $\text{TM@Si}_{12}$  cluster? 3) How does oxygen affect the geometric and electronic structures?

To shed light on the above questions, we perform first-principles calculations to probe the interaction of an oxygen molecule with the  $\text{W@Si}_{12}$  cluster, which has been previously reported to possess the largest HOMO–LUMO gap and the highest binding energy (18 electrons) among all of the  $\text{TM@Si}_{12}$  clusters [13–17]. The rest of the Letter is organized as follows: in Section 2, we describe the calculation method. The results and discussion are presented in Section 3, and finally we draw our main conclusions in Section 4.

## 2. Method

Spin-polarized calculations were carried out using the Vienna *ab initio* simulation package (VASP) [27] with the exchange–correlation energy correction described by the Perdew–Burke–Ernzerhof [28] parameterization. The interaction between the ions and valence electrons is described by the PAW potential [29]. The wave functions are expanded in a plane wave basis with an energy cut-off of 400 eV. As we used a simple cubic cell with a large lattice constant of 15 Å, only the  $\Gamma$  point was selected for the Brillouin zone integration. In the self-consistent field calculations, the accuracy is converged up to  $10^{-4}$  eV. The atomic positions were optimized by the conjugate gradient (CG) [30] method, with the force convergence set to 0.02 eV/Å, these convergence criteria can guarantee the accuracy of the total energy reaches to  $10^{-3}$  eV/atom. To investigate the adsorption behavior of the  $\text{O}_2$  molecule on  $\text{W@Si}_{12}$ , we first optimized the structures of the  $\text{W@Si}_{12}$  cluster and the isolated  $\text{O}_2$ , respectively; and then the whole structure by initially setting the oxygen molecule 4.0 Å away from the  $\text{W@Si}_{12}$  cluster. Various possible reaction paths were tested by the placement of the  $\text{O}_2$  around different sites of the  $\text{W@Si}_{12}$  cluster with different  $\text{O}_2$  orientations. Comparison of the total energies of these optimized clusters leads to the final product geometry of  $\text{O}_2\text{-W@Si}_{12}$ . By using the improved nudged elastic band [31] method with four interaction images, we systematically investigated the minimum energy path (MEP) of the adsorption process. The above method and model have been verified to be of sufficient accuracy to describe the adsorption behavior of  $\text{O}_2$  molecules on  $\text{Si}_n$  [6] and  $\text{Ba}_n$  [32] clusters in our previous calculations.

## 3. Results and discussion

First, we optimized the geometric structures of the  $\text{W@Si}_{12}$  cluster with many initial configurations, including some low symmetry candidates where the W atom resides on the cluster surface as generated by high temperature molecular dynamics, and some high symmetry structures, such as HP-W@ $\text{Si}_{12}$ , the anti-hexagonal prism (AHP) cage and FPF-W@ $\text{Si}_{12}$ . Our results show that the W atom prefers to reside at the cluster center, leading to five stable

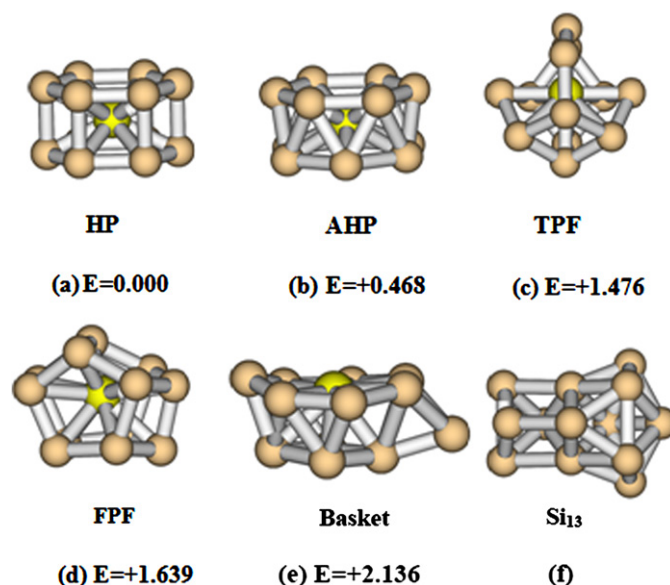


**Fig. 1.** (Color online.) The most stable structure and low-lying isomers of the  $\text{W@Si}_{12}$  cluster are shown in (a)–(e), and marked with relative energies (in eV). HP: hexagonal prism; AHP: anti-hexagonal prism; TPF: two pentagonal face; FPF: four pentagonal face; and Basket structures are presented. For comparison, the most stable structure of  $\text{Si}_{13}$  cluster is also shown in (f). The Si atoms are in orange, and the W atom in yellow.

**Table 1**

Formation energy of  $\text{W@Si}_{12}$  cluster,  $E_f = -(E(\text{W@Si}_{12}) - 12E(\text{Si}_{\text{atom}}) - E(\text{W}_{\text{atom}}))$  (eV). For the case of  $\text{Si}_{13}$ ,  $E_f = -(E(\text{Si}_{13}) - 13E(\text{Si}_{\text{atom}}))$  (eV). The average W–Si bond length,  $R(\text{W–Si})$  (Å) and the HOMO–LUMO gap,  $E_{\text{gap}}$  (eV) for the ground state and the low-lying isomers of the  $\text{W@Si}_{12}$  cluster. The formation energy,  $E_f = -(E(\text{HP-W@Si}_{12}) - E(\text{Si}_{12}) - E(\text{W}_{\text{atom}}))$  ( $E_f = -(E(\text{Si}_{13}) - E(\text{Si}_{12}) - E(\text{Si}_{\text{atom}}))$ ) for a single W (Si) atom reacting with the ground state structure of  $\text{Si}_{12}$  (Ref. [6]), leading to the ground state structure of HP-W@ $\text{Si}_{12}$  ( $\text{Si}_{13}$ ) is also presented.

$\text{W@Si}_{12}$	PAW–PBE			PAW–PW91		
	$E_f$	$R_{\text{W–Si}}$	$E_{\text{gap}}$	$E_f$	$R_{\text{W–Si}}$	$E_{\text{gap}}$
HP	53.679	2.664	1.411	54.513	2.665	1.392
AHP	53.211	2.672	1.145	53.953	2.676	1.139
TPF	52.203	2.692	1.230	53.079	2.697	1.223
FPF	52.040	2.656	0.342	52.864	2.658	0.265
$\text{Si}_{13}$	48.680	–	1.050	49.404	–	1.043
$\text{W} + \text{Si}_{12}$	8.484	–	–	7.660	–	–
$\text{Si} + \text{Si}_{12}$	3.506	–	–	2.706	–	–

W-encapsulated Si cages, as seen in Fig. 1 and Table 1. Among those, the HP-W@ $\text{Si}_{12}$  is the most stable, see Fig. 1(a), which is in close agreement with previous reports [12–17,25]. Relative to the formation (binding) energy of 48.680 eV for the most stable pure  $\text{Si}_{13}$  cluster (see Fig. 1(f), Ref. [6]), the HP-W@ $\text{Si}_{12}$  possesses a significantly larger value of 53.679 eV; the calculated formation energy ( $E_f = -(E(\text{HP-W@Si}_{12}) - E(\text{Si}_{12}) - E(\text{W}_{\text{atom}}))$ ) is 8.484 eV for a single W atom reacting with the ground state structure of  $\text{Si}_{12}$  (Ref. [6]), leading to the structure of HP-W@ $\text{Si}_{12}$ . However, the formation energy of a single Si atom reacting with the most stable structure of  $\text{Si}_{12}$  is merely 3.506 eV, producing the most stable  $\text{Si}_{13}$ , Fig. 1(f). Note also that the HOMO–LUMO gap (which in DFT calculations are generally underestimated and thus we emphasize are qualitative) of the HP-W@ $\text{Si}_{12}$  cluster, at 1.414 eV, is larger than that of the  $\text{Si}_{13}$  cluster, at 1.050 eV. All of this data indicates that the stability of HP-W@ $\text{Si}_{12}$  is enhanced, relative to that of the  $\text{Si}_{13}$  cluster. The optimized AHP-W@ $\text{Si}_{12}$  cluster (which is the next lowest in energy) is obtained by rotating one hexagonal ring 30 degree relative to the other along the sextuple axis of  $D_{6h}$  HP-W@ $\text{Si}_{12}$ , and is 0.468 eV less stable than the HP configuration, Fig. 1(b).

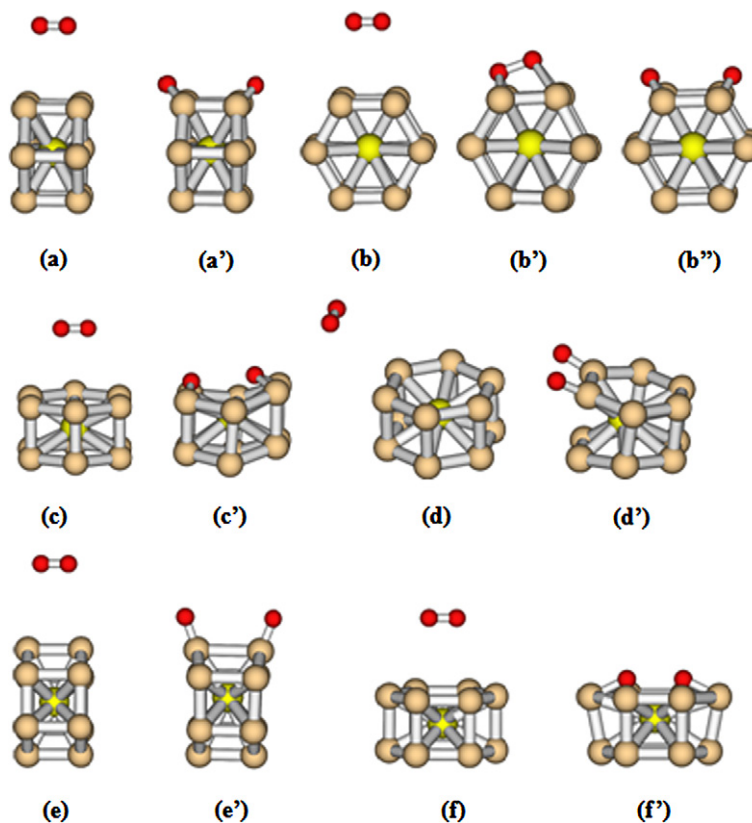


**Fig. 2.** (Color online.) (a)–(f) Six initial adsorption sites for the  $O_2$  molecule on the HP-W@Si<sub>12</sub> cluster while (a')–(f') correspond to the respective final configurations.

As presented in Fig. 1(c), among other low-lying isomers of the W@Si<sub>12</sub> cluster is one which is very similar to that reported by Hiura et al. [12], about 0.163 eV lower in energy than the FPF-W@Si<sub>12</sub> structure shown in Fig. 1(d). In this structure, there are only two pentagonal faces – for simplicity, we name it the TPF-W@Si<sub>12</sub> structure. In our calculations, the TPF-W@Si<sub>12</sub> cluster is spin-singlet with a significant  $E_{\text{gap}}$  as large as 1.230 eV. However, the FPF-W@Si<sub>12</sub> is spin-triplet and possesses a small  $E_{\text{gap}}$  of 0.342 eV due to spin-splitting. We emphasize that in Fig. 1(e), the W atom is only partially surrounded by Si atoms, and this low-lying isomer structure is very similar to that of the ground state basket configuration of the Ti@Si<sub>12</sub> cluster calculated by Kawamura et al. [24]; however, it is 2.136 eV higher in energy than HP-W@Si<sub>12</sub>. Other isomers with the W atom occupying the cluster surface are very unstable and hence are not shown here. In fact, we have also optimized these structures with a PAW-PW91 potential for comparison, as shown in Table 1. One observes that both PAW-PBE and PAW-PW91 calculations obtained the same relative stability order for these structures, with almost the same  $R(\text{Si}-\text{W})$  bond lengths and  $E_{\text{gap}}$ , although the PAW-PW91 method finds slightly larger formation energies. In later sections, we use the PAW-PBE potential for accuracy in describing the molecular adsorption.

Considering the highly symmetric configuration of the HP-W@Si<sub>12</sub> cluster, we selected six possible initial adsorption sites for single  $O_2$  molecule adsorption, as presented in Fig. 2. It is noted that in all these six cases, the  $O_2$  molecule possesses very small adsorption energy on the cluster ( $E_{\text{ads}}$  ranging from 0.004 to 0.027 eV, Table 2) if the initial distance between the center of the mass of the  $O_2$  molecule and the cage surface is larger than 3.5 Å. This result shows that there is no bonding between  $O_2$  and the cluster according to PBE calculations. In the final configuration, both  $O_2$  and the silicon cage remain intact and the system is in the triplet state due to the paramagnetic property of the  $O_2$  molecule.

**Table 2**

Adsorption energy for  $O_2$  molecule chemisorption on the HP-W@Si<sub>12</sub> cluster,  $E_{\text{ads}} = -(E(O_2/\text{HP-W@Si}_{12}) - E(O_2) - E(\text{W@Si}_{12}))$  (eV); the values in the bracket denote a weak molecular adsorption;  $R(\text{Si}-\text{O})$  (Å) and  $E_{\text{gap}}$  (eV) denote the average Si–O bond length and the HOMO–LUMO gap for the  $O_2/\text{HP-W@Si}_{12}$  product;  $E_{\text{bar}}$  (eV) and  $R(\text{O}-\text{O})$  (Å) correspond to the energy barrier for  $O_2$  dissociation and the O–O bond length at the saddle point (the values in the bracket are obtained by spin-conservation calculations).

Sites	$E_{\text{ads}}$ (eV)	$R_{\text{Si-O}}$ (Å)	$E_{\text{gap}}$ (eV)	$E_{\text{bar}}$ (eV)/ $R_{\text{O-O}}$ (Å)
(a)	(0.009) 6.252	1.708	1.155	0.736/1.316 (0.960/1.346)
(b)	(0.004) 0.970	2.082	1.275	0.456/1.265 (0.734/1.339)
(–)	6.088	1.703	1.162	0.016/1.512
(c)	(0.027) 5.597	1.781	0.931	0.672/1.327 (0.755/1.363)
(d)	(0.008) 4.039	1.542	1.344	0.474/1.319 (0.593/1.328)
(e)	(0.020) 3.673	1.547	0.473	0.601/1.244 (0.881/1.293)
(f)	(0.026) 2.832	1.726	1.002	1.102/1.344 (1.188/1.345)

However, if pushed gradually toward the HP-W@Si<sub>12</sub> cluster, the  $O_2$  molecule dissociates on the W@Si<sub>12</sub> cage once the distance between the  $O_2$  and the cluster surface is reduced to 2 Å, resulting in a product structure that is in the singlet state. Note that this activation process is practically possible only if in very high temperature and/or high pressure conditions, indicating the high inertness of the cluster to  $O_2$ . According to the order of adsorption energy for  $O_2$  dissociative adsorption on the HP-W@Si<sub>12</sub> cluster, the initial (final) configurations for these six cases are shown from Fig. 2(a) ((a')) to Fig. 2(f) ((f')), respectively, with path (a) showing the largest adsorption energy of 6.252 eV and path (f) the smallest of 2.832 eV, see Table 2.

An exception is case (b), in which the  $O_2$  first adsorbs as a molecule on the cage with an O–O bond length of 1.483 Å and an  $E_{\text{ads}}$  of 0.970 eV, Fig. 2(b') and Table 2. We note that structure (b') is nonmagnetic, and the  $O_2$  molecule adsorbs on the cage asymmetrically with two short Si–O bonds of 1.937 Å and two long Si–O bonds of 2.227 Å, respectively, indicating a strong chemisorption.

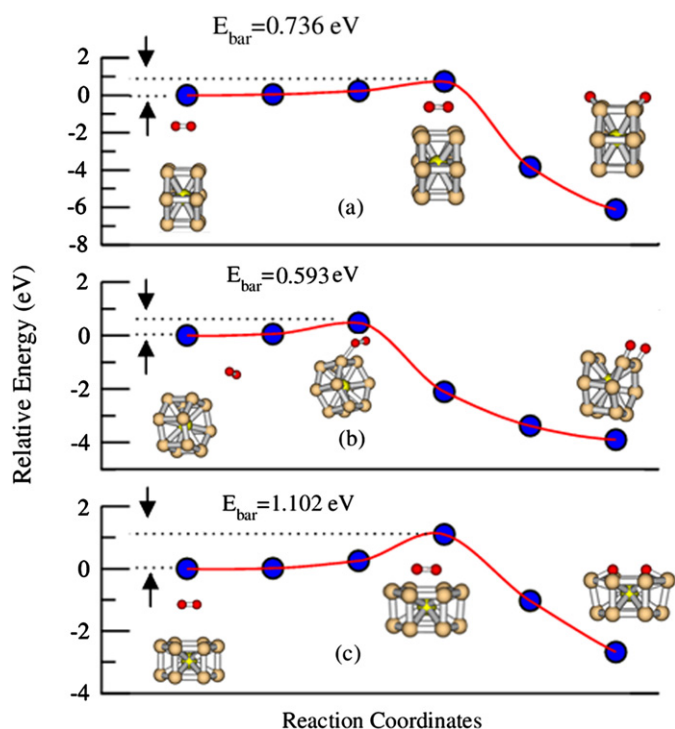


**Fig. 3.** (Color online.) Minimum energy path (MEP) obtained by NEB calculations for  $O_2$  dissociation on the HP-W@Si<sub>12</sub> cluster. (a), (b) and (c) correspond to the reaction with an initial adsorption site presented in Figs. 2(a), 2(d) and 2(f), respectively.

As one may expect, an introduction of a weak perturbation (about 0.016 eV, see later parts) induces the adsorbed  $O_2$  molecule to dissociate, resulting in the structure of (b''), lowering the total energy by 5.118 eV, relative to configuration (b').

As presented in Fig. 2 and Table 2, from a thermodynamic point of view, it is surprising to note that the favorite adsorption site for  $O_2$  on HP-W@Si<sub>12</sub> is located by the side of the cage, Fig. 2(a), rather than above the center of the hexagonal ring, Fig. 2(f), where the W metal atom is half encapsulated. In fact, the smallest adsorption energy is obtained at the (f) site. This suggests that geometry is not the only factor responsible for the inertness of the HP-W@Si<sub>12</sub> structure, though many previous investigations indicate that TM@Si<sub>12</sub> clusters (including HP-W@Si<sub>12</sub>) may be stabilized by a geometric effect, i.e., the TM atom encapsulated in the silicon cage is surrounded by twelve Si atoms and thus loses its reactivity. Thus, we deduce that the high inertness of W@Si<sub>12</sub> as well as its surprising inactivity toward  $O_2$  may originate from its unique electronic structure, which will be further analyzed in another paper [33].

Using the improved nudged elastic band [31] method with four interaction images, we have systematically investigated the minimum energy path (MEP) of the adsorption process, for all six cases. The O–O bond lengths in the saddle points and the corresponding kinetic energy barriers,  $E_{\text{bar}}$ , are shown in Table 2. For simplicity, only three representative MEPs are shown in Figs. 3(a), 3(b) and 3(c), corresponding to the initial adsorption sites in Figs. 2(a), 2(d) and 2(f), respectively. As mentioned above, it seems that the  $O_2$  molecule prefers to react with the HP-W@Si<sub>12</sub> cage from edge sites, say (a) and (d), rather than the unfavorable site (f), which is further confirmed by the MEP calculations: from site (d) ((a)), the energy barrier ( $E_{\text{bar}}$ ) is 0.474 (0.736) eV, whereas from site (f), it is 1.102 eV.

One may note that in the case of (c), the  $O_2$  is also initially located above the center of the hexagonal ring, and may dissociate by overcoming a small energy barrier of 0.672 eV. However, we stress that, firstly, the  $O_2$  adsorption energy difference between

cases (c) and (a) is 0.655 eV, and secondly the  $O_2$  dissociation barriers from the initial adsorption sites (b), (d) and (e) are significantly lower than that from (c): 0.456, 0.474 and 0.601 eV, respectively. Therefore, we conclude that  $O_2$  prefers to interact with the HP-W@Si<sub>12</sub> cluster from the sites beside the cage, such as (a), (b), (d), or (e), rather than above the center of the hexagonal ring. As aforementioned, finite and infinite TM@Si<sub>12</sub> tubes have been synthesized and may be used as nano-devices. Here, our prediction indicates that in air and at high temperature conditions,  $O_2$  molecules may react with the tube walls, but not with the tube edges that may be already saturated by hydrogen atoms, which is in stark contrast to the case of  $O_2$  reaction with carbon nanotubes, where the preference is the edge sites [34].

To further understand the mechanism of the interaction, we studied the electronic structure evolution of the HP-W@Si<sub>12</sub> cage during  $O_2$  adsorption and reaction, particularly the effect of oxygen on the geometric and electronic properties. Fig. 4 presents the electronic density of states (DOS) evolution for  $O_2$  dissociation on the HP-W@Si<sub>12</sub> cage from the initial adsorption site (a). It is shown that upon  $O_2$  dissociative adsorption, the average W–Si bonds increase from 2.664 to 2.676 Å, Table 2, and the HP cage also enlarges correspondingly. From the DOS in Fig. 4, it is seen that in the initial state ( $O_2$  molecule is about 3.5 Å away from the cage surface), there is almost no significant hybridization between the molecular states of  $O_2$  and those of the silicon cage. However, in the transition states, the energy levels become significantly complex and there are hybridizations between the  $2p\pi^*$  ( $2p\pi$ ) level of the adsorbed  $O_2$  species with the silicon states. In particular, the DOS of the final state also clearly indicates the strong hybridization of the Si–O bonds, though the states of the W atom are only slightly affected by the oxygen, due to the minor distortion of the Si cage and associated minor changes in the Si–W interactions. Interestingly, we note that the  $O_2$  changes from triplet to a singlet in the transition state ( $R(O-O) = 1.316$  Å), indicating activation of the  $O_2$  species. Such reaction is very similar to that of  $O_2$  with pure Si<sub>n</sub> clusters [6]. We also emphasize that, in the cases of dissociative adsorption, the oxygen states are occupied deep below the Fermi level, and there is no oxygen defect state in the HOMO–LUMO gap of the HP-W@Si<sub>12</sub> cage, as shown in the final column of Fig. 4.

We note that all the above calculations are performed in the framework of non-conservation of spin, i.e., in the initial stage, the system of  $O_2 + W@Si_{12}$  with large separation distance is in a spin-triplet state, but the product of reaction is spin-singlet. Experimentally, upon photoexcitation, the spin-triplet  $O_2$  molecules can be changed to a spin-singlet state, leading to the subsequent spin-singlet reaction products. However, in the absence of photoexcitation, this is a spin-forbidden reaction. Thus, spin-conserved calculations must be performed to correctly estimate the dissociation barrier for  $O_2$  molecule on W@Si<sub>12</sub> cluster. Correspondingly, we first performed spin-conserved (the system is kept as spin-triplet state) NEB calculations on the three representative cases, (a), (d) and (f), see Fig. 2, to identify their kinetic processes, respectively. For the case of (a), the bond length of the  $O_2$  molecule in the transition state is 1.346 Å, slightly larger than the value of 1.316 Å obtained in the spin-unconserved case. However, the dissociation barrier is significantly increased, by 0.224 eV; for the case of (d), a larger barrier of 0.593 eV is also identified, while for the case of (f), at the saddle point the dissociation barrier is also slightly increased by about 0.086 eV, becoming 1.188 eV. Motivated by the above test, we have also performed spin-conserved NEB calculations on all the other remained cases: (b), (c) and (e). The results show that the dissociation barrier is 0.734, 0.755, and 0.881 eV, for case (b), (c), and (e), respectively, and the O–O bond length ( $R_{O-O}$ ) is significantly increased in the saddle point, see Table 2, compared with the results from non-conservation

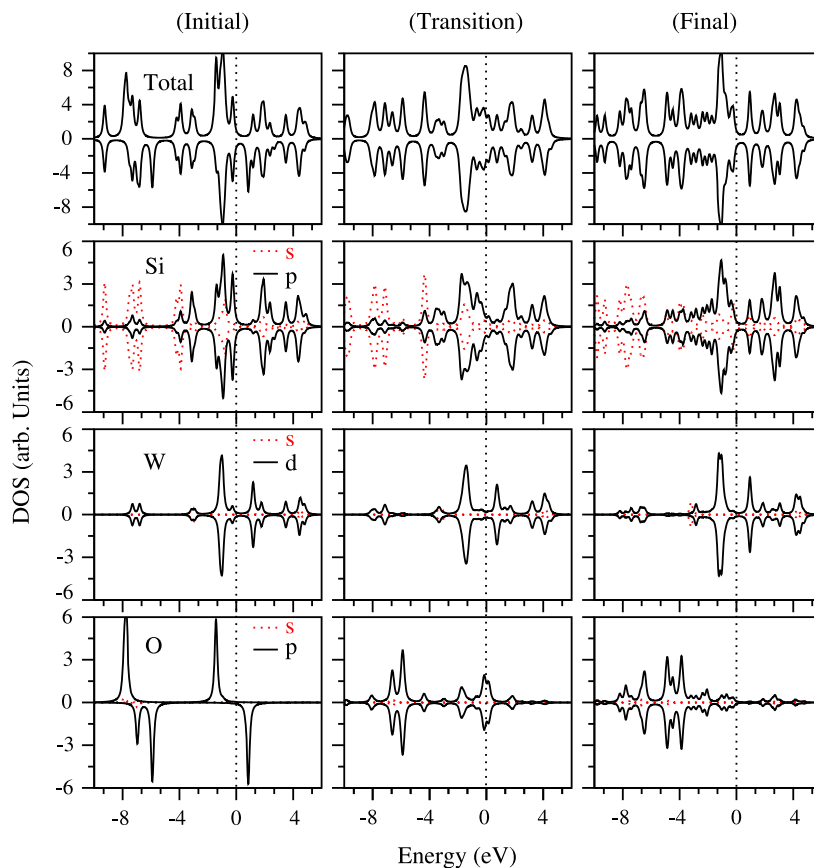


**Fig. 4.** (Color online.) Total and projected electronic density of states (PDOS) for  $O_2$  dissociative adsorption on the HP-W@Si<sub>12</sub> cluster with a path (a) presented in Fig. 3. (Initial), (Transition), and (Final) correspond to the initial state, transition state, and the final reacted product state, respectively. Fermi level has been shifted to zero, as denoted by the dotted line.

calculations. Note also that for the case of (b), in spin-unconserved calculations,  $O_2$  molecule can first molecularly chemisorb on the cluster surface, see (b'), however, in the spin-conserved calculations,  $O_2$  molecule directly dissociates on the cluster by overcoming a barrier of 0.734 eV from the initial weak adsorption state with the  $O_2$  species intact. These results imply again that the spin state of  $O_2$  molecule may play a key role in the reaction process.

Finally, we stress other factors that may also count for the inertness of W@Si<sub>12</sub> cluster. First, it is well known that in general the inertness of a cluster is HOMO–LUMO gap dependent, i.e., the larger the HOMO–LUMO gap, the higher its stability. However, the present calculations may generally underestimate the HOMO–LUMO gap compared to the experimental values, due to the well-known limitation of the current DFT calculation level. Therefore, in the realistic case, the dissociation barrier may be even larger than the calculated values. On the other hand, in realistic case, large energy barrier (about 1.0 eV) should be conquered to excite  $O_2$  molecule to a spin-singlet state from the ground state of spin-triplet state [35]. However, in our DFT calculations the excitation energy for such a transition seems to be significantly underestimated (see Table 2, the barrier difference between spin-conserved and spin-unconserved calculation is fairly small), may due to the limitation of the current DFT calculation. Alternatively, excitation W@Si<sub>12</sub> cluster to a spin-triplet state may also readily trigger the chemical reaction between W@Si<sub>12</sub> cluster and  $O_2$  molecule, however, such excitation energy is 1.242 eV in our current calculations. Another important factor is that initially,  $O_2$  can merely weakly adsorb on the HP-W@Si<sub>12</sub> cluster with a very shallow potential well (several tens meV), and thus the reaction barrier for  $O_2$  on the cluster obtained by both spin-constraint and spin-nonconstraint

NEB calculations is dramatically larger than the desorption barrier, rendering the high inertness of W@Si<sub>12</sub> cluster toward  $O_2$  reaction in the framework of winger's spin rule. These discussions are very helpful to understand the inertness of HP-W@Si<sub>12</sub> toward  $O_2$  molecules and other oxidation process at ambient temperature.

#### 4. Summary

First-principles calculations have clarified the electronic structure and stability of the W@Si<sub>12</sub> cluster under  $O_2$  molecule adsorption and reaction. Our results show that the W-encapsulated Si<sub>12</sub> hexagonal prism cage is very inert to oxidation. The  $O_2$  molecule only weakly adsorbs onto the cluster at relatively low temperatures, in the range of several tens meV. However, significant reaction barriers (0.593–1.118 eV) for the  $O_2$  molecule on the cluster are identified on different adsorption sites, nevertheless, these reaction paths are spin forbidden reactions according to Winger's spin selection rule. These results imply that  $O_2$  readily desorb from the cluster surface rather than dissociate and oxidize the W@Si<sub>12</sub> cluster upon excitations. In high temperature and high pressure conditions, the  $O_2$  molecules may dissociate on the preferential edge site by overcoming a significantly large energy barrier.

#### Acknowledgements

This work is completed on the High Performance Clusters Center of Zhengzhou University. S.F.L. gratefully acknowledges the supports by the National Science Foundation of China under Grants No. 10604049 and 11074223. This work was partly supported by the EPSRC under a Platform Grant (GR/S52636/01, EP/E046193/1).

## References

- [1] H.W. Kroto, J.R. Heath, S.C. O'Brien, R.F. Curl, R.E. Smalley, *Nature (London)* 318 (1985) 162.
- [2] M.F. Jarrold, E.C. Honea, *J. Phys. Chem.* 95 (1991) 9181.
- [3] K.-M. Ho, A.A. Shvartsburg, B. Pan, Z.-Y. Lu, C.-Z. Wang, J.G. Wacker, J.L. Fye, M.F. Jarrold, *Nature (London)* 392 (1998) 582.
- [4] K.A. Jackson, M. Horoi, I. Chaudhuri, T. Frauenheim, A.A. Shvartsburg, *Phys. Rev. Lett.* 93 (2004) 013401.
- [5] J. Bai, L.-F. Cui, J. Wang, S. Yoo, X. Li, J. Jellinek, C. Koehler, T. Frauenheim, L.-S. Wang, X. Zeng, *J. Phys. Chem. A* 110 (2006) 908.
- [6] S.F. Li, X.G. Gong, *J. Chem. Phys.* 122 (2005) 174311, and the references [1–19] therein.
- [7] R.L. Zhou, B.C. Pan, *J. Chem. Phys.* 128 (2008) 234302.
- [8] V. Kumar, Y. Kawazoe, *Phys. Rev. Lett.* 90 (2003) 055502.
- [9] S.M. Beck, *J. Chem. Phys.* 90 (1989) 6306; S.M. Beck, *J. Chem. Phys.* 87 (1987) 4233.
- [10] S.M. Beck, *Adv. Met. Semicond. Clusters* 1 (1993) 241.
- [11] V. Kumar, Y. Kawazoe, *Phys. Rev. Lett.* 87 (2001) 045503; V. Kumar, Y. Kawazoe, *Phys. Rev. B* 65 (2002) 073404.
- [12] H. Hiura, T. Miyazaki, T. Kanayama, *Phys. Rev. Lett.* 86 (2001) 1733.
- [13] N. Uchida, T. Miyazaki, T. Kanayama, *Phys. Rev. B* 74 (2006) 205427, and the references therein.
- [14] J. Lu, S. Nagase, *Phys. Rev. Lett.* 90 (2003) 115506; P. Sen, L. Mitás, *Phys. Rev. B* 68 (2003) 155404.
- [15] T. Miyazaki, H. Hiura, T. Kanayama, *Phys. Rev. B* 66 (2002) 121403(R).
- [16] J. Ulises Reveles, S.N. Khanna, *Phys. Rev. B* 72 (2005) 165413.
- [17] S.N. Khanna, B.K. Rao, P. Jena, *Phys. Rev. Lett.* 89 (2002) 016803.
- [18] J. Ulises Reveles, S.N. Khanna, *Phys. Rev. B* 74 (2006) 035435.
- [19] L.J. Guo, G.F. Zhao, Y.Z. Gu, X. Lu, Z. Zeng, *Phys. Rev. B* 77 (2008) 195417.
- [20] W.R. Creasy, A. O'keefe, J.R. McDonald, *J. Phys. Chem.* 91 (1987) 2848.
- [21] M.F. Jarrold, U. Ray, K.M. Creegan, *J. Chem. Phys.* 93 (1990) 224; D.E. Bergeron, A.W. Castleman Jr., *J. Chem. Phys.* 117 (2002) 3219.
- [22] A.A. Gnidenko, V.G. Zavodinsky, *Semiconductors* 42 (2008) 800.
- [23] M. Ohara, K. Koyasu, A. Nakajima, K. Kaya, *Chem. Phys. Lett.* 371 (2003) 490.
- [24] H. Kawamura, V. Kumar, Y. Kawazoe, *Phys. Rev. B* 70 (2004) 193402.
- [25] T. Miyazaki, H. Hiura, T. Kanayama, *Eur. Phys. J. D* 24 (2003) 241; P. Sen, L. Mitás, *Phys. Rev. B* 68 (2003) 155404; G. Mpourmpakis, G. Froudakis, A.N. Andriotis, M. Menon, *J. Chem. Phys.* 119 (2003) 7498; A.K. Singh, T.M. Briere, V. Kumar, Y. Kawazoe, *Phys. Rev. Lett.* 91 (2000) 146802.
- [26] C. Xiao, F. Hagelberg, W.A. Lester Jr., *Phys. Rev. B* 66 (2002) 075425; A.K. Singh, T.M. Briere, V. Kumar, Y. Kawazoe, *Phys. Rev. Lett.* 91 (2000) 146802; A.A. Saranin, et al., *Nano Lett.* 4 (2004) 1469; A.K. Singh, V. Kumar, et al., *Nano Lett.* 2 (2002) 1243.
- [27] G. Kresse, J. Furthmüller, *Phys. Rev. B* 54 (1996) 011169; G. Kresse, J. Furthmüller, *Comput. Mater. Sci.* 6 (1996) 15.
- [28] J.P. Perdew, K. Burke, M. Ernzerhof, *Phys. Rev. Lett.* 77 (1996) 3865.
- [29] P.E. Blöchl, *Phys. Rev. B* 50 (1994) 17953; G. Kresse, D. Joubert, *Phys. Rev. B* 59 (1999) 1758.
- [30] M.P. Teter, M.C. Payne, D.C. Allan, *Phys. Rev. B* 40 (1989) 12255.
- [31] G. Henkelman, B.P. Uberuaga, H. Jónsson, *J. Chem. Phys.* 113 (2000) 9901; G. Henkelman, H. Jónsson, *J. Chem. Phys.* 113 (2000) 9978.
- [32] S.F. Li, Xinlian Xue, G. Chen, D.W. Yuan, Yu Jia, X.G. Gong, *J. Chem. Phys.* 124 (2006) 224711.
- [33] S.F. Li, et al., to be submitted for publication.
- [34] X.Y. Zhu, S.M. Lee, Y.H. Lee, T. Frauenheim, *Phys. Rev. Lett.* 85 (2000) 2757.
- [35] G. Herzberg, *Molecular Spectra and Molecular Structure: Spectra of Diatomic Molecules*, vol. 1, 2nd ed., D. van Nostrand Company, Inc., Toronto, 1950.